REAPPRAISING THE PRODUCTION AND TRANSFER OF HYDROGEN TO THE UPPER ATMOSPHERE AT TIMES OF ELEVATED WATER VAPOR

F. Montmessin, *LATMOS/IPSL, UVSQ Université Paris-Saclay, Sorbonne Université, CNRS, Guyancourt, France,* **D. A. Belyaev,** *Space Research Institute of the Russian Academy of Sciences (IKI RAS), Moscow, Russia,* **F. Lefèvre,** *LATMOS, Sorbonne univ. Paris France,* **J. Alday,** *Open University, Milton Keynes, U.K.*, **M. Vals,** *LATMOS, Guyancourt,* **A. A. Fedorova, O. I. Korablev, A. V. Trokhimovskiy,** *IKI Moscow,* **M. S. Chaffin, N. M. Schneider,** *LASP, Boulder, Colorado, United States*

Introduction: Water escape on Mars has recently undergone a paradigm shift with the discovery of unexpected seasonal variations in the population of hydrogen atoms in the exosphere where thermal escape occurs and results in water lost to space. This discovery led to the hypothesis that, contradicting the accepted pathway, atomic hydrogen in the exosphere was not only produced by molecular hydrogen but mostly by high altitude water vapor. Enhanced presence of water at high altitude during southern spring and summer, due to atmospheric warming and intensified transport, favors production of H through photon-induced ion chemistry of water molecules and thus appears to be the main cause of the observed seasonal variability in escaping hydrogen (Chaffin et al., 2014; 2017; Clarke et al., 2014, Heavens et al., 2018). This hypothesis is supported by the large concentrations of water vapor observed between 50 km and 150 km during the southern summer solstice and global dust events (Fedorova et al., 2020; 2021, Belyaev et al., 2021; Aoki et al., 2019). Using a simplified air parcel transport model, we have explored the formation of H from water photolysis from 40 to 80 km and its vertical advection to the upper atmosphere. Comparing the injection modes of a variety of events (global dust storm, perihelion periods, regional storm), we conclude that southern spring/summer controls H production and further ascent into the upper atmosphere on the long term with direct implication for water escape.

Model Description: The assumption that H production above 80 km dominates from an escape standpoint should be revisited by considering the nature of transport (advection, not diffusion) and the contribution of the atmosphere below. In that context, a different perspective would look at the fate of a wet air parcel lifted from near the ground and progressively carried to an altitude range where H atoms are produced and then diffuse up the exobase. This supposes to adopt a Lagrangian standpoint, where one tracks over time (i.e., altitude) the changing gaseous composition inside the parcel.

To this end, we have employed a hybrid approach combining observational results, photochemistry and transport diagnostics from a 3D Mars climate model to represent the processes affecting the composition of an air parcel over time. The rationale for this simplified approach is that the entire representation of H production, evolution, and transport cannot be based solely on observations or the 3D model. This approach of mixing observations and modeling was introduced and used by Alday et al. (2021) to establish the prevalence of the southern spring/summer in the annual H production of the middle atmosphere.

Observations can only indirectly constrain the velocity of ascent in the middle atmosphere (Heavens et al., 2019), but they can constrain directly water vapor, pressure and temperature, which are the main parameters to model the relevant photochemistry. On the other hand, given the current maturity of Mars climate models (Navarro et al., 2014; Haberle et al. 2019; Neary et al., 2020), using their transport diagnostics is a relevant option for specifying the range of vertical wind speeds needed for our model.

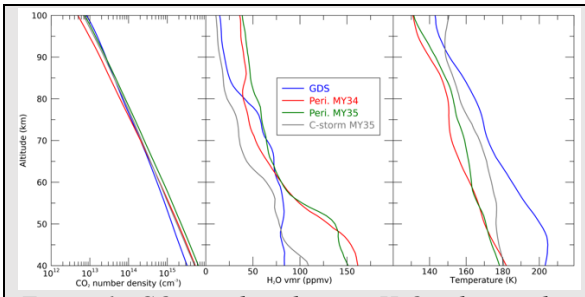

Figure 1: CO_2 number density, H_2O relative abundance and temperature derived from ACS data by Belyaev et al. (2021) for the four cases investigated in this study: MY34 GDS, Perihelion, MY35 Perihelion and C-storm.

Our hybrid model tracks the fate of a wet atmospheric parcel undergoing ascent and chemistry, using the observed water vapor profiles reported in Belyaev et al. (2021) and the chemical model of Lefèvre et al. (2004) whose latest version has been presented in Lefèvre et al. (2021). We aim at tracking the variation in H number density (N_H) inside the parcel during its ascent to the upper atmosphere at times of intensified upward transport, i.e., during perihelion and during the MY34 GDS. The parcel ascends at a velocity ω of 10 cm/s as derived from the Mars Climate database (Millour et al., 2017).

Dataset: One can distinguish between two modes of high-altitude water vapor migration: periodic and stochastic. The periodic mode relates to perihelion conditions as it occurs every year at the same period of time and is only driven by the reproducible evolution of the southern spring/summer

climatic conditions, except when affected by the occurrence of a GDS such as in MY28. The stochastic mode corresponds to the unpredictable occurrences of dust storms, whose impact on climate is large-scale. This concerns global dust storms, and large-scale A-, B-, C- storms. Both periodic and stochastic modes occur only during the second half of the year, and it is now widely accepted that only southern spring and summer contribute to water vapor migration to the upper atmosphere (Alday et al., 2021).

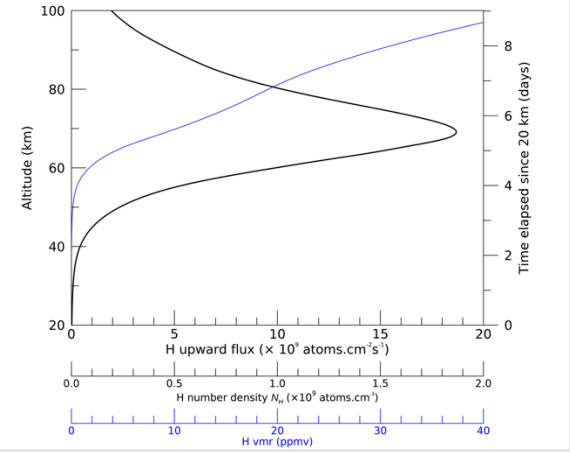

Figure 2: Model results for the H number density in the parcel (NH) and the resulting upward flux for the MY34 perihelion case (black solid line).

Ls periods tested. We selected the same periods of time as Belyaev et al. (2021) to which we added the MY35 C-storm period from the same dataset (see Figure 1). We thus based our simulations on data collected during the climax of the MY34 GDS (195°-220°), near perihelion (Ls 270°) in MY34 and MY35, as well as during the MY35 C-storm (Ls 320°). We discarded the option to present a simulation for the MY34 C-storm (Ls 330°) because this event was not sufficiently well covered to allow a meaningful evaluation of the H atom transfer at that time. Therefore, we conducted four simulations. Results were obtained for a particular latitude range that theoretically corresponds to the main zone of H ascent (i.e., 60°S for Perihelion and C-Storm, 0° for the GDS).

Results:

MY34 Perihelion. Here we consider the particular situation occurring during the transition between southern spring and summer and that is henceforth referred to as the Perihelion season and that encompasses the period from L_s 240° to 270°. Alday et al. (2021) demonstrated the prevalence of the Perihelion season for the formation of H and D atoms at 60 km of altitude. This conclusion was based on applying theoretical photolysis rates upon HDO and H_2O profiles observed by ACS. *Figure 2* shows the altitude (or equivalently time, on the right axis) evolution of the hydrogen number density (N_H) in the air parcel and the corresponding upward flux (equal to $N_H \times \omega$). N_H shows a pronounced peak of 1.9×10^9 atoms.cm^{-3} at 69 km that is reminiscent of the net production peak found at 65 km. However, N_H then decreases after rising above the peak as subsequent H production diminishes and cannot compensate dilution subsequent to the parcel volume expansion. At 80 km, we find that the upward hydrogen flux is of 1.1×10^{10} cm^{-2}s^{-1}, a value that is nearly twice the net photolysis product of H integrated from 80 to 100 km. The H flux at the bottom of the upper atmospheric domain is not only significant, it actually accounts for a dominant portion of the H budget in the upper atmosphere of the southern summer, when H is known to escape massively.

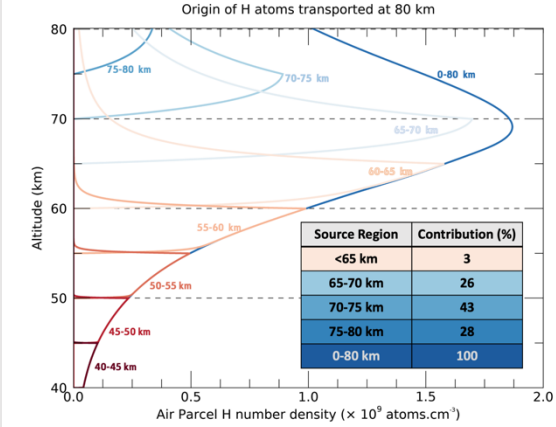

Figure 3: Predictions for a set of configurations where production only occurs in a 5 km-thick layer whose top altitude vary from 45 to 80 km. Plotted quantity is the parcel H number density.

Hydrogen origin in the lower atmosphere. Our air parcel model can be used to track the origin of the H atoms advected to 80 km (*Figure 3*). To do so, we restrict production inside 5-km atmospheric layers located between 40 and 80 km (*Figure 3*). Our model confirms that no H atoms produced below 60 km can access the upper atmosphere as they are bound to recombine before reaching 80 km, which implies that almost no atoms produced in the peak production region contribute to escape. After being advected from their production zone below 60 km, H atoms are completely lost after 1 or 2 km of ascent. The production zone that matters for escape comprises altitudes from 65 to 80 km, with a dominant contribution from the 70 to 75 km region.

Result Comparison. The MY34 configuration described above has revealed the main characteristics of the H migration phenomenon, showing the significance of the H flux at 80 km and the partitioning of the H origin among the atmospheric layers located below and in particular between 60 and 80 km. We then subsequently applied our model to the three other configurations of interest: MY35 Perihelion, MY34 GDS and MY35 C-storm (see *Figure 1* and *Figure 4*). Due to TGO's orbit constraints, a large

part of the MY34 C-storm was not monitored by ACS. The data gap actually covered the peak activity of this regional storm, which implies our results would have largely underestimated the C-storm upward flux, explaining our choice to solely focus on the C-storm event of MY35. Yet, this event produced an intense brightening of the hydrogen corona (Chaffin et al., 2021). In addition, the MY34 GDS/Perihelion, as well as the MY35 Perihelion cases also suffer from a 5 to 10° sampling gap that happened around their climax. However, because these gaps are relatively short when compared to the duration of these events and affected all of the main events (GDS and Perihelion) in the same way, their significance is likely to be small and their effect cannot bias the interpretation of one over the other.

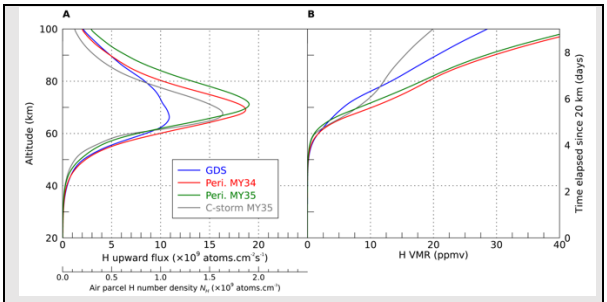

Figure 4: A synthesis of the four configurations explored with the air parcel model: MY34 GDS/Perihelion, and MY35 Perihelion/C-storm. (A) H Upward flux and concentration in the parcel during its rise from 20 to 100 km. (B) Same as (A) except NH is converted into H vmr (ppmv).

MY34 and MY35 Perihelion cases are in remarkable agreement, both exhibiting the same upward flux profile (*Figure 4*) with a pronounced peak around 70 km only slightly shifted upward in MY35. This altitude offset explains why the MY35 80 km H flux is ~30% larger than MY34, as a higher proportion of H atoms are produced closer to the 80 km boundary. Indeed, water vapor is 15 ppmv more abundant in MY35 at 80 km, which then directly impacts H production and upward flux. These results support the idea that the perihelion configuration is highly reproductible from year to year, which provides confidence for extrapolating its contribution in the escape budget on a longer term.

The GDS case exhibits a H flux profile that is significantly flared compared to the perihelion case, reflecting the distinct H_2O vmr profile of the GDS that shows a nearly uniform mixing ratio of ~70 ppmv below 70 km. The GDS H flux has a maximum value located at 65 km that is twice smaller than for perihelion cases. At 80 km, GDS flux remains distinctly smaller than the two perihelion seasons considered here. However, at 85 km, the GDS flux catches up with MY34 Perihelion flux. The broadened peak of the GDS implies that a larger proportion (~50%) of the H population origin is located close to the 80 km boundary. In addition, the total density of the MY34 GDS above 80 km is higher than for perihelion cases (*Figure 4*), which mitigates the volume expansion (dilution) effect on the air parcel in this altitude range.

The MY35 C-storm case produces a H upward flux profile resembling that produced for perihelion, likely in response to a circulation pattern that is a remnant of the solstitial configuration, with a single cell whose strength was recharged by the momentary surge of dust. Its peak flux is located 5 km below the flux peak of perihelion, yet is twice greater than that of the GDS. However, both events end up generating the same flux at 80 km.

Upward flux vs. neutral photolysis. We compared the upward H flux in terms of hydrogen input into the region above 80 km, with the direct deposition of hydrogen from water photolysis above 80 km. On the case of MY34 perihelion, the upward flux is about twice the net column production of H atoms out of photolysis between 80 and 100 km. For other cases, we found the following: (i) for MY35 perihelion, the upward flux was 55% greater than local photolysis production, (ii) for the MY34 GDS, the upward flux was 30% greater, and (iii) for the MY35 C-storm, the upward flux was more than twice the local production. These results imply that the upward influx of H at the bottom of the upper atmospheric domain is the dominant supplier in the context of the neutral photochemistry.

H production type in column rate (atoms per $cm^{-2}s^{-1}$)		**Event type**			
		Perihelion		**MY34 Global Dust Storm**	**MY35 C-storm**
		MY34	**MY35**		
H_2-CO_2^+ chemistry		1.6×10^8 (k19)		1.6×10^8 (k19)	1.6×10^8 (k19)
H_2O-CO_2^+ chemistry		1×10^9 (k19)		2.4×10^9 (s20)	
This study	**H_2O photolysis (80-100 km)**	5×10^9	7.5×10^9	5.4×10^9	3.7×10^8
	H upward flux	1×10^{10}	1.3×10^{10}	8.4×10^9	8.1×10^9

Table 1: a synthesis of the results obtained in this study and compared with other works (k19: Krasnopolsky, 2019; s20: Stone et al., 2020).

Discussion: Assuming that the H atoms crossing the 80 km boundary can be then carried up to escape altitudes, our results shed light on the potential of each event for hydrogen escape. Table 1 summarizes the production rates computed for most of the events discussed here and for the various H production modes that have been studied so far. Of all the processes involved in the production and injection of H atoms into the upper atmosphere, the upward transfer is found to be systematically greater than production from water photolysis or ion chemistry. This statement is only valid outside the cold aphelion period, where H_2 molecules are the main precursor of H atoms.

This raises the question of the fate of H atoms crossing the 80 km boundary. Shaposhnikov et al. (2022) explore the dynamical mechanisms that carry

volatiles into the upper atmosphere at GDS and perihelion times. Using a Mars' GCM to address the gravity wave breaking effect on global circulation and the transport of water at high altitude, they show that atmospheric updrafts are the main carrier of volatiles up to 100 km, above which molecular diffusion combines with advection and then controls above 120 km the ascent of gases to the exobase. It is therefore legitimate to apply our advective transport model to hydrogen atoms produced below 80 km. Since the lifetime of hydrogen atoms increases steadily with altitude, once they have entered the upper atmospheric domain above 80 km, they are likely to reside there long enough for a significant fraction of them to reach the exobase. In fact, the way circulation is organized at times of high water events implies a massive upwelling either at the equator (GDS) or at high southern latitudes (perihelion) compensated by a massive downwelling at the pole(s). During perihelion, the MCD indicates that the downwelling velocity is twice larger than upwelling (1.7, not shown, vs. 0.7 m/s maximum values) yet is confined into a narrow band at the north pole. Our air parcel concept only captures the ascent part of the hydrogen journey into the upper atmosphere. At 100 km, that is at the top of our model, molecular diffusion will then take over the rest of the ascent that will lead released H atoms to escaping altitude. Yet a fraction of these atoms will eventually return to the middle atmosphere via the downwelling region.

Conclusion: We have used a 1D hybrid model to represent the ascent of a wet air parcel at times of intense dust and transport activity. This model combines observations of the ACS instrument that measured, for the first time, water vapor abundance from 20 to 120 km. These observations enable the in-depth study of how the water vapor penetration to high altitude contributes to hydrogen production above 80 km. In contrast with other 1D models that have been used to explore Mars' photochemistry, our model represents the vertical transport through advection with a constant velocity of 10 cm/s up to 100 km. Our results imply that, contrary to a common assumption made in models used to study Mars' photochemistry and escape processes, the region between 60 and 80 km cannot be neglected in the production and migration of hydrogen to the upper atmosphere. In particular, these results imply that upper atmosphere photochemistry models intending to capture Southern Summer conditions need to carefully consider the flux boundary condition for H at the lower boundary if it is higher than 80 km. Testing a variety of configurations, from the MY34 GDS to the recent MY35 perihelion period, we have been able to assess how the hydrogen upward flux from above 60 km varies with events. Stochastic events (GDS and A, B, C- storms) have a strong imprint on the escape budget, but our results suggest perihelion remains the dominant escape component on the long term.

References:

Alday, et al. (2021). *Nature Ast.*. https://doi.org/10.1038/s41550-021-01389-x

Aoki, S., et al. (2019). *J. of Geophys. Res.: Planets*. https://doi.org/10.1029/2019JE006109

Belyaev, D. A., et al. (2021). *Geophys. Res. Let.*. https://doi.org/10.1029/2021GL093411

Chaffin, M. S., et al. (2014). *Geophys. Res. Let.*. https://doi.org/10.1002/2013GL058578

Chaffin, M. S., et al. (2017). *Nature Geos.*. https://doi.org/10.1038/ngeo2887

Clarke, J. T., et al. (2014). *Geophys. Res. Let.*. https://doi.org/10.1002/2014GL061803

Fedorova, A. A., et al. (2020). *Science*. https://doi.org/10.1126/science.aay9522

Fedorova, A. A., et al. (2021). *J. of Geophys. Res.: Planets*. https://doi.org/10.1029/2019JE006109

Haberle, R. M., et al. (2019). *Icarus*. https://doi.org/10.1016/j.icarus.2019.03.026

Heavens, N. G., et al. (2018). *Nature Ast.*. https://doi.org/10.1038/s41550-017-0353-4

Krasnopolsky, V. A. (2019). *Icarus*, https://doi.org/10.1016/j.icarus.2018.10.033

Lefèvre, F., et al. (2004). *J. of Geophys. Res.: Planets*. https://doi.org/10.1029/2004JE002268

Lefèvre, F., et al. (2021). *J. of Geophys. Res.: Planets.* https://doi.org/10.1029/2021JE006838

Millour, E., et al. (2017). The Mars Climate Database. https://doi.org/10.1016/j.icarus.2014.12.034

Navarro, T., et al.. (2014). *J. of Geophys. Res.: Planets*. https://doi.org/10.1002/2013JE004550

Neary, L., et al. (2020). *Geophys. Res. Let.*. https://doi.org/10.1029/2019GL084354

Shaposhnikov, D.S., et al. (2022). *J. of Geophys. Res.: Planets*. https://doi.org/10.1029/2021JE007102

Stone, S. W., et al. (2020). *Science*. https://doi.org/10.1126/science.aba5229